A NOVEL DISCRETE PARTICLE MODEL
OF BLAST FURNACE IRONMAKING PROCESS

Qin-Fu HOU,[1,2*] **Dian-Yu E,**[1] **Shi-Bo KUANG,**[1] **Zhao-Yang LI,**[1] **and Ai-Bing YU**[1]

[1] Laboratory for Simulation and Modelling of Particulate Systems, Department of Chemical Engineering, Monash University, Clayton, VIC 3800, AUSTRALIA

[2] Laboratory for Simulation and Modelling of Particulate Systems, School of Materials Science and Engineering, The University of New South Wales, Sydney, NSW 2052, AUSTRALIA

*Corresponding author, E-mail address: Qinfu.Hou@monash.edu

ABSTRACT

The blast furnace (BF) with high temperatures and high pressures is one of the key reactors consuming major portion of energy in iron and steelmaking. Even slight improvement of its energy efficiency can generate huge benefits to the reduction of cost and more importantly to the mitigation of its carbon footprint on environment. Currently, there are mainly two groups of approaches for the understanding of the black box reactor. One group is based on continuum models, requiring relatively less computational effort. However, the closure constitutive correlations for the multiphase flow are not well established. The other group is based on discrete particle models. The discrete approaches can overcome the requirement of constitutive correlations of solid phase and treat grains of particulate raw materials individually using Newton's law of motion. It is desirable to develop a discrete particle model to address in-furnace thermo-chemical behaviours in the BF. This work presents a novel discrete particle model by which the interphase heat and mass transfer and key chemical reactions are considered. It can predict key features in the BF such as the formation of different flow zones. This work establishes a framework towards a virtual experimental BF.

INTRODUCTION

The blast furnace (BF) is the work-horse of ironmaking process with the current development of technology although there are some alternatives using smelting and direct reduction. In the BF process, iron-bearing materials (e.g., lump iron ore and pellet) and coke are charged into the top of the BF. The charged solids flow downward under the gravity and interact with the counter current gas introduced from tuyeres. In this process the charged solids descend and experience intensive heat load, chemical reactions and phase transformation. The process is quite complicated under high temperatures (~2,000°C) and high pressures (around two times of ambient pressure) and it is largely a black box operation. Furthermore the BF process represents ~70% of CO_2 emission of an integrated steel plant while the iron and steelmaking industrial contributes ~30% to the total of industrial emissions. It is of high significance to understand the process for improving its energy efficiency and hence reducing carbon footprint of iron and steel industry on environment.

The understanding and prediction of the BF process can be achieved by experimental and numerical approaches. Due to the complicated multiphase flow in the BF it is hard to investigate in-furnace phenomena and to comprehensively examine the effects of various operational factors and material properties. There is only one experimental BF in operation by Luossavaara-Kiirunavaara Aktiebolag (LKAB) and the data provided is limited due to high cost (Dahlstedt et al., 1999). Generally, this difficulty can be overcome by numerical approaches. There are mainly two groups of numerical approaches with different advantages and limitations. One group treats different phases as continua and solves the governing equations for heat and mass transfer and chemical reactions (Dong et al., 2007). Such continuum approaches are suitable for large scale simulation with less computational demand. However, it is not easy to obtain accurate input conditions and to obtain useful information at a particle scale. The other group under development treats charged solids as discrete phase and reducing gas as continuous phase based on the so-called combined computational fluid dynamics (CFD) and discrete element method (DEM) approach (Zhu et al., 2007; 2008). Such a combined approach can vary material properties readily. With the fast development of numerical techniques and computer technology it is expected that this approach can be extended to large scale simulation of the BF process in the near future.

There are various investigators using the combined CFD-DEM approach in the study of the BF process as reviewed by Ariyama et al. (2014). However, the efforts are mainly focused on the gas-solid flow in model BF for the understanding of the effects of raceway and cohesive zone shapes. The predetermination of the raceway size and the shape of cohesive zone are rather arbitrary as heat transfer and chemical reactions are not considered. Recently only a few studies are dedicated to heat transfer and chemical reactions in a simplified geometry such as a cylindrical moving bed. There is no prediction of the complicated heat transfer and the reduction of iron ore and hence the dynamic in-furnace features with real BF geometry.

This work presents a novel BF model at a particle scale implemented with heat transfer and chemical reaction models. The transient process in the BF with the geometry similar to that of LKAB experimental BF is predicted. It can be an alternate platform for the understanding of the

BF ironmaking process for its control and the improvement of energy efficiency.

MODEL DESCRIPTION

This work presents a discrete particle model of the BF process involving discrete solids (iron ore and coke) and a continuum phase (reducing gas). It is formulated on the combined CFD-DEM approach (Xu and Yu, 1997; Feng and Yu, 2004; Zhou et al., 2010; Hou et al., 2012c). An in-house code for the BF is extended to include heat and mass transfer models (Zhou et al., 2009; Hou et al., 2012b; 2012a; 2015). Major reaction models are also adopted for the examination of thermo-chemical behaviours, as used in continuum approaches (Dong et al., 2007; Kuang et al., 2014).

Governing equations for solid phase

The motion of solids is described by the DEM. Thus a particle has translational and rotational motions. The interaction between the particle and its neighbouring particles and/or walls can occur through which the momentum and energy exchange takes place. At any time t, the governing equations of the motions of particle i of mass m_i and radius R_i are written as:

$$m_i \, dv_i/dt = \sum_j (\mathbf{f}_{e,ij} + \mathbf{f}_{d,ij}) + \mathbf{f}_{pf,i} + m_i \mathbf{g}, \quad (1)$$

and

$$I_i \, d\boldsymbol{\omega}_i/dt = \sum_j (\mathbf{T}_{t,ij} + \mathbf{T}_{r,ij}), \quad (2)$$

where $\mathbf{v}_i$ and $\boldsymbol{\omega}_i$ are the translational and rotational velocities, and $I_i \, (= 2/5 m_i R_i^2)$ is the moment of inertia of the particle. Particle-fluid interaction force $\mathbf{f}_{pf,i}$, the gravitational force $m_i\mathbf{g}$ and the forces between particles (and between particles and walls) are involved. The forces between particles include the elastic force $\mathbf{f}_{e,ij}$ and viscous damping force $\mathbf{f}_{d,ij}$. The torque acting on particle i due to particle j includes two components: $\mathbf{T}_{t,ij}$, which is generated by the tangential force and causes particle i to rotate; and $\mathbf{T}_{r,ij}$, which, commonly known as the rolling friction torque, is generated by the asymmetric normal contact forces and slows down the relative rotation between contacting particles (Zheng et al., 2011). For possible multiple interactions of particle i, the interaction forces and torques between each pair of particles are summed up. Most of the equations to determine the forces and torques are well recorded in the literature as, for example, reviewed by Zhu et al. (2007). The equations used in our previous studies (Zhou et al., 2010; Hou et al., 2012c) are adopted for the present work.

Particle i exchanges heat in three modes: by convective heat transfer with surrounding fluid, by conductive heat transfer to other particles or walls, and by radiative heat transfer to its nearby environment. The governing equations of energy balance and species concentration for particle i is written as:

$$m_i c_{p,i} \, dT_i/dt = \sum_j \dot{Q}_{i,j} + \dot{Q}_{i,f} + \dot{Q}_{i,rad} + \dot{Q}_{i,wall}, \quad (3)$$

$$m_i \, dC_{i,m}/dt = s_{i,m}, \quad (4)$$

where $\dot{Q}_{i,j}$ is the heat exchange rate between particles i and j by conduction; $\dot{Q}_{i,f}$ is the heat exchange rate between particle i and its local surrounding fluid by convection; $\dot{Q}_{i,rad}$ is the heat exchange rate between particle i and its local surrounding environment by radiation; and $\dot{Q}_{i,wall}$ is the heat exchange rate between particle i and wall by conduction. Mathematically, Eq. (3) is the same in expression as the lumped-capacity formulation, where the thermal resistance within a particle is neglected (Incropera and Dewitt, 2002). This condition is valid when the Biot number, defined as $h \cdot (V_i/A_i)/k_{pi}$, is less than 0.1, where h is heat transfer coefficient; V_i is particle volume; A_i is particle surface area; and k_{pi} is particle thermal conductivity. However, this equation here is established on the basis of energy balance at the particle scale and it is valid if the representative values of parameters are properly set at this scale (Zhou et al., 2009). $C_{i,m}$ is the concentration of species m in particle i and $s_{i,m}$ is the reaction rate of species m with surrounding environment.

The equations for the calculation of heat exchange rates in Eq. (3) are well documented (see, for example, Table 1 in Hou et al., 2012a), and not given here for brevity.

Governing equations for gas phase

The continuum gas phase is modelled similarly to the one widely used in the conventional two-fluid model (Anderson and Jackson, 1967). According to Zhou et al. (2010), there are three formulations (Sets I, II and III) and Set I can be used generally. In this work, Set I is used. Thus, the conservations of mass and momentum in terms of the local averaged variables over a computational cell are given by:

$$\partial(\rho_f \varepsilon_f)/\partial t + \nabla \cdot (\rho_f \varepsilon_f \mathbf{u}) = 0, \quad (5)$$

and

$$\partial(\rho_f \varepsilon_f \mathbf{u})/\partial t + \nabla \cdot (\rho_f \varepsilon_f \mathbf{u}\mathbf{u}) = -\nabla p - \mathbf{F}_{fp} + \nabla \cdot \boldsymbol{\tau} + \rho_f \varepsilon_f \mathbf{g}. \quad (6)$$

The corresponding energy equation for heat transfer can be written as:

$$\partial(\rho_f \varepsilon_f c_{pf} T)/\partial t + \nabla \cdot (\rho_f \varepsilon_f \mathbf{u} c_{pf} T) = \nabla \cdot (k_e \nabla T) + \dot{Q}. \quad (7)$$

The species transport equation for different gas components can be written as:

$$\partial(\rho_f \varepsilon_f Y_i)/\partial t + \nabla \cdot (\rho_f \varepsilon_f \mathbf{u} Y_i) = \nabla \cdot (\varepsilon_f \Gamma_i \nabla Y_i) + R_i + S_i, \quad (8)$$

where $\mathbf{u}$, ρ_f, p and $\mathbf{F}_{fp}$ are the fluid velocity, density, pressure and volumetric fluid-particle interaction force, respectively; $\boldsymbol{\tau}$ and ε_f are the fluid viscous stress tensor and porosity respectively. Note that ε_i is the local porosity for particle i for calculating particle-fluid drag force and ε_f is determined over a CFD cell. k_e is the fluid thermal conductivity. The volumetric particle-fluid interaction force $\mathbf{F}_{fp}$ in Eq. (6) can be determined as $\mathbf{F}_{fp} = \sum_{i=1}^{k_v} (\mathbf{f}_{d,i} + \mathbf{f}_{pg,i})/\Delta V$. The volumetric heat exchange rate $\dot{Q}$ in Eq. (7) is determined as $\dot{Q} = \sum_{i=1}^{k_v} (\dot{Q}_{f,i} + \dot{Q}_{f,wall} + \dot{Q}_{f,rad})/\Delta V$, where $\dot{Q}_{f,i}$ is the heat exchange rate between fluid and particle i by convection; $\dot{Q}_{f,wall}$ is the heat exchange rate between fluid and a wall by convection; and $\dot{Q}_{f,rad}$ is the heat exchange rate between fluid and its environment by radiation. Because the emissivity of fluid is low, the heat transfer between fluid and its environment by radiation is ignored. This

work considers one continuum gas phase and Y_i is the concentration of species i. R_i is the production rate of i by chemical reactions and S_i is the reaction rate with discrete phase which equals to the sum of s_i over all particles in a CFD cell. Γ_i is the diffusion coefficient of species i.

Chemical reaction rates for major reactions considered are based on one interface unreacted core model, as used by Kuang et al. (2014). The chemical reactions considered include reduction of iron ore by CO or H_2, solution-loss reaction between coke and CO_2, direct reduction and water gas reactions. The calculation equations for chemical reduction rates are selected according to reduction degree of iron ore.

The numerical method for CFD-DEM simulations is well documented (Xu and Yu, 1997; Feng et al., 2004; Zhou et al., 2010). The same coupling scheme is used here as before, and not given here for brevity.

SIMULATION CONDITIONS

The present work aims to establish a virtual experimental BF. Hence, the geometry is set according to that of LKAB experimental BF, as given in **Figure 1**(a). The mesh size shown in **Figure 1**(b) has been examined, and the results do not improve much if a finer mesh is used.
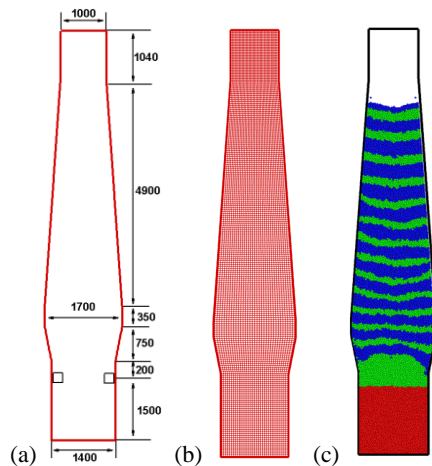
Figure 1: (a) Geometry of the model BF according to LKAB experimental BF, (b) the CFD mesh, and (c) initial charged solids (green for coke particles, blue for iron ore particles, and red for particles in the hearth).

The gas composition set at the inlet is the same to that obtained through mass and heat balance (Kuang et al., 2014). The solids charged in the present model include coke and iron ore, and their properties are given in Table 1. The layered structure of the initial state is given in Figure 1(c), indicated by different colours for different types of solids. The hearth is filled with high temperature particles without chemical reactions considered. It is worth to note that this treatment allows us to partially consider the effect of liquid hot metal in hearth. By fixing a high temperature for the particles in hearth the function of hearth as a heat reservoir is considered to some degree. Nonetheless, the effect of chemical reactions relevant to liquid hot metal is not considered. This treatment should be further justified and improved in the future to fully address the effect of liquid hot metal.

The multi-stage simulation procedure is described here. First, the BF is charged with coke particles, which is consistent with practical operation. Then, the coke particles will be discharged from raceway regions at a given rate (determined as a number of particles per second), resembling the coke combustion at raceway regions. At the same time, iron ore and coke particles with the same number of discharged particles will be charged at the top alternatively with the ambient temperature (25°C), forming a layered structure and a stable stock line. Thirdly, heat transfer models are introduced when the flow patter reaches a macroscopically steady state. Finally, chemical reaction models are introduced when the average temperature of all particles reaches 1200°C (this time is set as the start point for result discussion). Completely reduced iron ore will be discharged when it reaches a temperature higher than that corresponding to the complete smelting of iron (assumed as 1400°C in the present study). At this stage, the charging rate equals to the sum of discharged coke particles at raceway regions and discharged iron ore particles.

Table 1: Physical properties of gas, iron ore and coke, and inlet gas composition and wall temperature.

Variables	Values
Number of particles (N), -	32,000
Particle diameter of iron ore/coke d_p, mm	40/40
Particle density of iron ore/coke ρ, kg/m³	3000/1081
Thermal conductivity of iron ore/coke k_p, W/(m·K)	80/1.70
Specific heat of iron ore/coke c_p, J/(kg·K)	600/850
Particle-particle/wall sliding friction μ_s, -	0.3
Particle-particle/wall rolling friction μ_r, mm	0.01d_p
Restitution coefficient, -	0.8
Particle Young's modulus E, kg/(m·s²)	1×10⁷
Particle Poisson ratio ν, -	0.3
Wall temperature, °C	25
Inlet gas temperature T_{in}, °C	2000
Inlet gas velocity, m/s	80
Fluid density ρ_f, kg/m³	1.2
Fluid molecular viscosity μ_f, Pa·s	1.8×10^{-5}
Fluid thermal conductivity k_f, W/(m·K)	2.62×10^{-2}
Fluid specific heat c_{pf}, J/(kg·K)	1000
Inlet gas composition, mole percentage	
$CO/CO_2/H_2/H_2O/N_2$	34.959/0/0.813/0/64.228

RESULTS AND DISCUSSION

The BF ironmaking process involves complicated multiphase thermo-chemical behaviours, usually proceeding at high temperatures and high pressures. This paper presents a particle scale model for the investigation of in-furnace behaviours. It will first present a comparison of the attained flow zones in a steady state with the observation of dissection studies (Omori, 1987). Then, it will illustrate the transient process with the introduction of heat transfer and chemical reactions, leading to the steady state from the initial charged solids. Finally, it will discuss the effect of raceway size on the formation of different regions.

As shown in Figure 2(a), the complicated distribution of flow zones was observed in dissection studies of BF. The charged solids (iron ore and coke) display a layered structure in the top with low temperatures. With the descending of the charged solids iron ore will be reduced by carbon mono-oxide or hydrogen, and the coke is consumed through solution-loss and water gas reactions.

When the iron ore reaches its softening and melting temperatures, a fused layer can be observed in the vicinity of cohesive zone. Below the cohesive zone there are the coke and deadman zone. Liquid iron percolates through the cohesive and the deadman zones into the hearth.
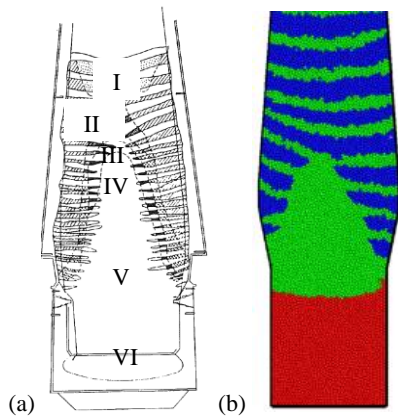

Figure 2: In-furnace pattern of different zones: (a) from dissection study (I: layered structure; II: fused layer; III: cohesive zone; IV: coke zone; V: deadman and VI: hearth) (adopted from Fig. 1.2 of the book by Omori (1987)) and (b) from particle scale simulation.

A similar pattern of different zones is reproduced by the present particle scale simulation as shown in Figure 2(b). The ore and coke layers will be stratified as they descend above the cohesive zone where ore particles start softening and melting. Reduced iron will percolate through the coke and deadman zone into the hearth. The predicted results agree well with the general understanding: (1) reducing gas will develop in the central part of the BF so that iron ore will be reduced quickly in the centre, thereby the deadman mainly composed of coke is formulated; the development of reducing gas in the central region is related to the loss of kinetic energy of gas jets from tuyeres; (2) the charged solids flow into the raceway regions through the funnel flow region in the BF, and because of this iron ore particles near the walls are reduced completely at a lower level than that in the central region.

The transient formation of different zones is illustrated in Figure 3 where the distribution of ore and coke particles and corresponding temperature is demonstrated. The initial state is shown at zero second. The bed temperature is slightly higher than that of steady state because chemical reactions will consume heat. The transient states at 200 and 400 seconds show the gradual formation of different zones. A steady state can be observed at around 430 seconds with a stable deadman and a distribution of temperature. In the present study, it is assumed that the smelting and softening process occurs in the temperature range of 1200~1400°C. The cohesive zone is highlighted in the distribution of temperature. It should be noted that the steady state is reached faster because larger reaction rates are adopted. The temperatures for the softening and smelting of iron ore, which can be determined through lab-scale experiments, can be adjusted for different material properties.
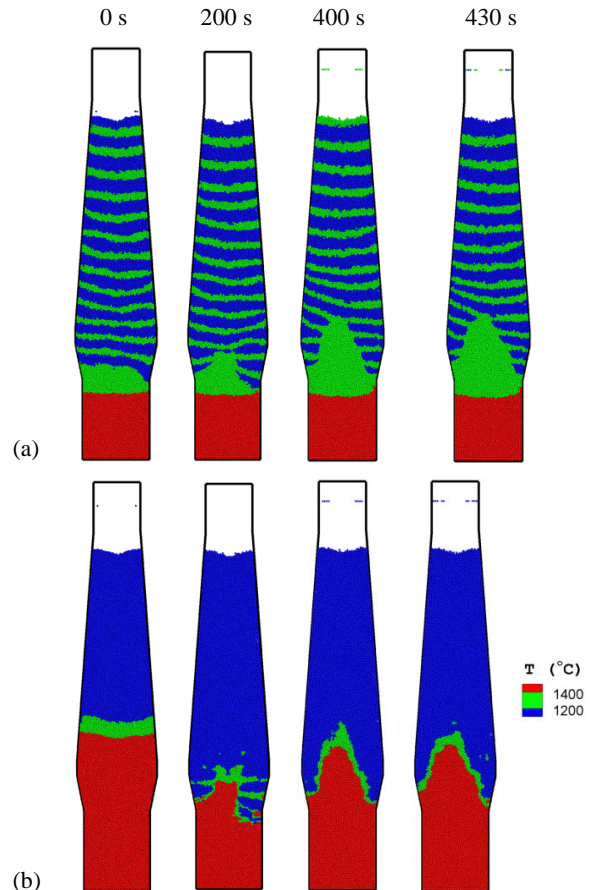
Figure 3: Transient formulation of different zones: (a) solids distribution (see Fig. 1 for colour code) and (b) temperature distribution.
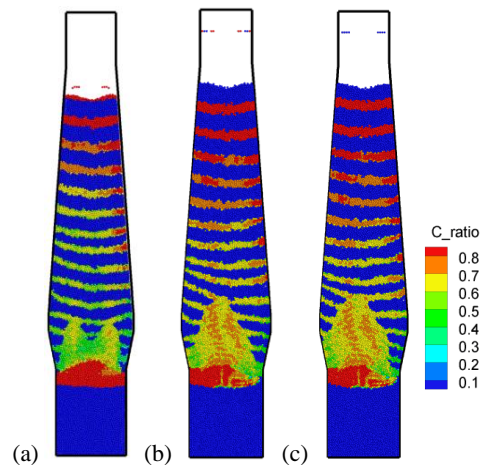
Figure 4: Flow zones in BF with different raceway sizes: $2d_p$ at 730 s (a) and $5d_p$ at 430 s (b) and 460 s (c). The percentage of carbon in each particle is indicated by C_ratio.

The raceway size and shape are critical factors of smooth operation and productivity, and they can vary with the change of blast rate, pulverized coal injection, and coke properties. The model in this work removes the coke particles in a square region at a given rate (Figure 1(a)). The effect of the raceway size on the final steady state is demonstrated for two raceway sizes in Figure 4. With the smaller raceway size an irregular shape of deadman is

4

observed, which is not stable. At this condition the slipping of charged solids could occur. With the larger raceway size an inverse 'v' shape of deadman is observed, which is desired and good for smooth operation. The raceway size varies complicatedly with material properties and operation conditions. Further effort should be made to investigate the in-furnace phenomena in connection with the shape and size of raceway.

Though the present model can reproduce several key in-furnace features of the complicated BF ironmaking process it has various treatments and simplifications. For example the shrinkage and phase transformation of iron ore and the combustion of coke at raceway regions should be further addressed. The softening and melting behaviours are not considered in this work and hence their effects on gas pressure drop in the cohesive zone are not discussed. Further model development will be realized and presented in future publications to overcome those treatments and simplifications.

CONCLUSIONS

A novel discrete particle model of the BF ironmaking process is developed and it can obtain particle scale information such as the reduction degree of iron ore, consumption of coke, and temperature field. The key features of different zones are dynamically reproduced such as the position and shape of the cohesive and the deadman zones and the layered structure. It can be used to investigate the effects of material properties on in-furnace behaviours for improving energy efficiency and operation. The model framework can also be extended to the study of thermo-chemical behaviours in similar processes such as fluidised beds and dryers.

ACKNOWLEDGEMENTS

REFERENCES

ANDERSON, T.B. and JACKSON, R., (1967), "Fluid mechanical description of fluidized beds-equations of motion". *Ind. Eng. Chem. Fund.*, 6, 527-539.

ARIYAMA, T., NATSUI, S., KON, T., UEDA, S., KIKUCHI, S. and NOGAMI, H., (2014), "Recent progress on advanced blast furnace mathematical models based on discrete method". *ISIJ Int.*, 54, 1457-1471.

DAHLSTEDT, A., HALLIN, M. and TOTTIE, M., (1999). LKAB's experimental blast furnace for evaluation of iron ore products. Proceedings of Scanmet 1, 235-245.

DONG, X.F., YU, A.B., YAGI, J.I. and ZULLI, P., (2007), "Modelling of multiphase flow in a blast furnace: Recent developments and future work". *ISIJ Int.*, 47, 1553-1570.

FENG, Y.Q., XU, B.H., ZHANG, S.J., YU, A.B. and ZULLI, P., (2004), "Discrete particle simulation of gas fluidization of particle mixtures". *AIChE J.*, 50, 1713-1728.

FENG, Y.Q. and YU, A.B., (2004), "Assessment of model formulations in the discrete particle simulation of gas-solid flow". *Ind. Eng. Chem. Res.*, 43, 8378-8390.

HOU, Q.F., LI, J. and YU, A.B., (2015), "CFD-DEM study of heat transfer in the reduction shaft of Corex". *Steel Res. Int.*, 86, 626-635.

HOU, Q.F., ZHOU, Z.Y. and YU, A.B., (2012a), "Computational study of the effects of material properties on heat transfer in gas fluidization". *Ind. Eng. Chem. Res.*, 51, 11572-11586.

HOU, Q.F., ZHOU, Z.Y. and YU, A.B., (2012b), "Computational study of the heat transfer in bubbling fluidized beds with a horizontal tube". *AIChE J.*, 58, 1422-1434.

HOU, Q.F., ZHOU, Z.Y. and YU, A.B., (2012c), "Micromechanical modeling and analysis of different flow regimes in gas fluidization". *Chem. Eng. Sci.*, 84, 449-468.

INCROPERA, F.P. and DEWITT, D.P., (2002). Fundamentals of Heat and Mass Transfer. John Wiley & Sons, New York.

KUANG, S.B., LI, Z.Y., YAN, D.L., QI, Y.H. and YU, A.B., (2014), "Numerical study of hot charge operation in ironmaking blast furnace". *Miner. Eng.*, 63, 45-56.

OMORI, Y., (1987). Blast Furnace Phenomena and Modelling. Elsevier Applied Science, London.

XU, B.H. and YU, A.B., (1997), "Numerical simulation of the gas-solid flow in a fluidized bed by combining discrete particle method with computational fluid dynamics". *Chem. Eng. Sci.*, 52, 2785-2809.

ZHENG, Q.J., ZHU, H.P. and YU, A.B., (2011), "Finite element analysis of the rolling friction of a viscous particle on a rigid plane". *Powder Technol.*, 207, 401-406.

ZHOU, Z.Y., KUANG, S.B., CHU, K.W. and YU, A.B., (2010), "Discrete particle simulation of particle-fluid flow: Model formulations and their applicability". *J. Fluid Mech.*, 661, 482-510.

ZHOU, Z.Y., YU, A.B. and ZULLI, P., (2009), "Particle scale study of heat transfer in packed and bubbling fluidized beds". *AIChE J.*, 55, 868-884.

ZHU, H.P., ZHOU, Z.Y., YANG, R.Y. and YU, A.B., (2007), "Discrete particle simulation of particulate systems: Theoretical developments". *Chem. Eng. Sci.*, 62, 3378-3396.

ZHU, H.P., ZHOU, Z.Y., YANG, R.Y. and YU, A.B., (2008), "Discrete particle simulation of particulate systems: A review of major applications and findings". *Chem. Eng. Sci.*, 63, 5728-5770.